# Accurate Modeling of Excitonic Coupling in Cyanine Dye Cy3

Mohammed I. Sorour,\*,† Kurt A. Kistler,\*,‡ Andrew H. Marcus,\*,¶ and Spiridoula

Matsika\*,†

†Department of Chemistry, Temple University, Philadelphia, Pennsylvania 19122, United
States

‡Department of Chemistry, Pennsylvania State University, Brandywine campus, Media,
Pennsylvania 19063, United States

¶Department of Chemistry and Biochemistry, University of Oregon, Eugene, OR 97403,

United States

E-mail: Mohammed.Sorour@temple.edu; kak46@psu.edu; ahmarcus@uoregon.edu; smatsika@temple.edu

#### Abstract

Accurate modeling of excitonic coupling in molecules is of great importance for inferring the structures and dynamics of coupled systems. Cy3 is a cyanine dye that is widely used in molecular spectroscopy. Its well-separated excitation bands, high sensitivity to the surroundings, and the high energy transfer efficiency make it a perfect choice for excitonic coupling experiments. Many methods have been used to model the excitonic coupling in molecules with varying degrees of accuracy. The atomic transition charge model offers a high-accuracy and cost-effective way to calculating the excitonic coupling. The main focus of this work is to generate high-quality atomic transition charges that can accurately model the Cy3 dye's transition density. The transition density of the excitation of the ground to first excited state is calculated using configuration-interaction singles and time-dependent density functional theory and benchmarked against the algebraic diagrammatic construction method. Using the transition density, we derived the atomic transition charges using two approaches: Mulliken population analysis and charges fitted to the transition electrostatic potential. The quality of the charges is examined, and their ability to accurately calculate the excitonic coupling is assessed via comparison to experimental data of an artificial biscyanine construct. Theoretical comparisons to the supermolecule ab initio couplings and the widely used point-dipole approximation are also made. Results show that using the transition electrostatic potential is a reliable approach for generating the transition atomic charges. A high-quality set of charges, that can be used to model the Cy3 dye dimer excitonic coupling with high-accuracy and a reasonable computational cost, is obtained.

## 1 INTRODUCTION

Cyanine dyes are widely used to label proteins and DNA. <sup>1–5</sup> Their high environmental sensitivity, unique spectral signatures, and bright spectra make them an ideal choice to monitor molecular dynamics as complicated as protein and RNA folding and with sensitivity to

capture the effects of changing temperature.<sup>2,5–10</sup> The Cy3 dye (the specific structure, 1,1'-dimethyl-3,3,3',3'-tetramethylindocarbocyanine, studied here is shown in Figure 1) is one of the most widely used fluorescent probes and has been the chromophore of choice for Protein Induced Fluorescence Enhancement and Förster Resonance Energy Transfer (FRET) experiments because of its high absorption coefficient, high photostability, and favorable quantum yield. <sup>1,8,9,11–17</sup>

The ability of Cy3 chromophores as multimers to probe the local conformations of biological macromolecules can be described by exciton theory. <sup>18,19</sup> The main mechanism used to explain the spectral lineshapes of absorbance and circular dichroism spectra is the excitonic coupling between chromophores which assumes that the photo-excitation is not localized on one chromophore but rather delocalized over all the participating monomers. <sup>20,21</sup> The excitonic coupling not only explains the spectral lineshapes, but also shows its dependence on the local dimer conformation. <sup>18,19,22–24</sup>

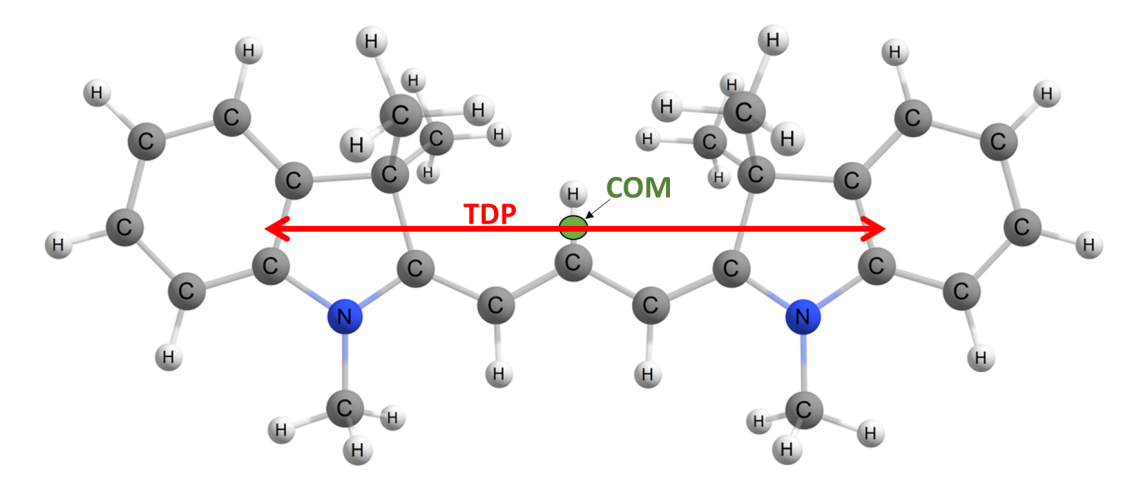


Figure 1: Structure of the Cy3 monomer optimized at B3LYP/6-31G(d)/(PCM=Water) level. The transition dipole moment, TDP, is represented by the red double headed arrow. The TDP is lying on the monomer's long axis. The center-of-mass (COM) is shown in green.

Quantum mechanically, the properties of two or more interacting monomers can be explained by their electronic interactions which would be preferably studied theoretically using high-level electronic structure *ab initio* calculations. Using high-level *ab initio* theory might not be feasible or practical to study the electronic structure of molecular aggregates com-

posed of large monomers like Cy3, especially if multiple dimer orientations are dynamically possible; one would need to balance and choose between cost and accuracy. The Frenkel exciton model<sup>22</sup> enables the description of the spectral properties of the coupled system using the individual chromophores' electronic properties and the interaction, or coupling between their individual vertical excitations. The electronic coupling accounts for the three main coupling contributors, namely the Coulomb coupling that accounts for the electronic transitions' interactions, the exchange coupling that accounts for the indistinguishability of the electrons in many-electron wave functions, and the orbital overlap of the electronic wavefunctions of the monomers. <sup>25,26</sup> In most cases, unless the inter-chromophore distance is extremely small or the electric transition dipole moment is zero, i.e. the monomer excitation is forbidden, the Coulomb coupling is the main contribution, so it is a good approximation to theoretically treat the electronic interaction with just this term and neglect the overlap and exchange terms. There have been many efforts to accurately model the Coulombic coupling as a representative of the electronic coupling. A numerically accurate and efficient method is to use the interaction between electronic transition charge densities of the excited state of chromophores. <sup>27,28</sup> Despite its high-accuracy, it does not perfectly serve the cost-effectiveness purpose of easing the excitonic coupling calculations, as it is a computationally intense model to implement. <sup>25</sup> In the transition density cube method, <sup>27,28</sup> the transition density of a chromophore is first calculated as a product of the electronic ground and excited state. Other approaches based on real time TDDFT have also been developed, and can be very efficiently applied to large systems. <sup>29,30</sup>

Considering the electronic transition density between two states in a similar way as we consider the electronic density of a single state, one can decompose the electronic transition density into point charges centered on the atomic centers via a variety of electronic structure methods.<sup>31</sup> Hence, the electronic coupling is simplified to a form that substitutes the classical partial charges of the classical Coulombic interaction equation with the atomic transition charges, (tqs). The transition charges can be obtained using several methods,

including the Mulliken population analysis, <sup>25,32–35</sup> as well as fitting charges to the transition electrostatic potential (trESP), where the latter uses the transition density matrix to generate the ESP. <sup>31,36,37</sup> Once we have the transition electrostatic potential, we can derive atomic transition charges using any of the available ESP fitting methods, such as Merz-Singh-Kollman (MK), Charges from Electrostatic Potential (CHELP), Charges from Electrostatic Potential-grid method (CHELPG), and restrained electrostatic potential (RESP). <sup>38–41</sup>

The point-dipole approximation (PDA) <sup>42–44</sup> is the simplest model for the electronic coupling of excited state, and has been widely used. In the point-dipole approximation, or the dipole-dipole approximation, the chromophores are represented by their transition dipole moments and the Coulombic coupling can be approximated as the dipole-dipole interaction between the transition dipoles of the monomers. The PDA is a very simple model to use, is highly sensitive to the individual chromophores' relative orientation, is very accurate at large separation distances where the coupling is considered to be weak, and is very efficient when multiple orientations are possible and necessary to consider. <sup>19,45–47</sup> Experimentalists have used the PDA model to extract geometrical information from coupled aggregate systems including those with Cy3 units. <sup>8,9,15–17,48–50</sup> The relatively large size of the Cy3 chromophore makes PDA a convenient model to use for calculating its supermolecule excitonic coupling in dimeric systems mainly because of the comparatively higher sophistication of the higher level approximations and due to the high computational cost of the *ab initio* methods.

The cost-effectiveness of the PDA model for big systems like Cy3 is limited by its accuracy. The PDA model is known to break down at the medium and strong coupling regimes, and at center-of-masses separation distances comparable to the chromophore's dimensions. <sup>19,29,51</sup> These pitfalls arise at these separation distances, mainly, because the transition dipole (TDP) of the PDA model fails to account for the full dimensionality of the chromophore and its transition density and, also, because of its inherent inability to account for the electronic overlap and exchange interactions. Hence, we would expect the PDA model to work well with the coupled Cy3 aggregates when the units are separated by distances larger than its

dimensions (Cy3's long axis is ~14 Å). Some PDA-based predictions suggest that the Cy3 units of a homodimer can exist in an interchromophoric separation distance range of 4 to 10 Å. 8,9,49,50 Relying on the PDA model for measuring the coupling and/or to predict geometrical information of coupled Cy3 units in such intermediate to small separation distances might provide incorrect results. Hence, it is advantageous to use a higher level approximation to model the excitonic coupling of aggregate systems with large subunits like Cy3. Other models have been proposed to solve the inability of the PDA to account for the physical dimensions of large chromophores, such as the extended-dipole model (EDM), 52 where the transition dipole moment is represented as two point charges of equal magnitude and opposite signs separated by the vector length.

The transition charge model offers a unique solution to account for much of the physical dimensionality of the system. The main objective of this paper is to generate a high-quality set of transition charges that can more accurately represent the magnitude, topography, and orientation of the transition density, and consequently the coupling. The ground to first excited state transition density matrix of Cy3 is obtained using configuration-interaction singles (CIS) and time-dependent density functional theory (TDDFT) with various functionals, and their basis set dependence is tested. The algebraic diagrammatic construction scheme through second order (ADC(2)) is used to benchmark the CIS and TDDFT transition density dipoles. The atomic transition charges are generated using the Mulliken and trESP treatments, and we determine the set of charges (LC-ωPBE/Def2SVP/trESP) that best reproduce their corresponding ab initio TDP magnitude and orientation as a metric to gauge approximation accuracy with the ab initio transition density. The performance of the homodimer couplings obtained electrostatically from atomic transition charges (tqs) are compared to those obtained from ab initio calculations on the supermolecule, which include overlap and exchange influences, as well as the PDA model. Finally, to further test the quality of the charges, the excitonic coupling of an experimentally well-studied biscyanine system is calculated, and the results show that the charges are able to capture the experimental excitonic coupling magnitude, as well as the influence of the dimer orientation geometries and solvent effects on the coupling.

## 2 METHODS

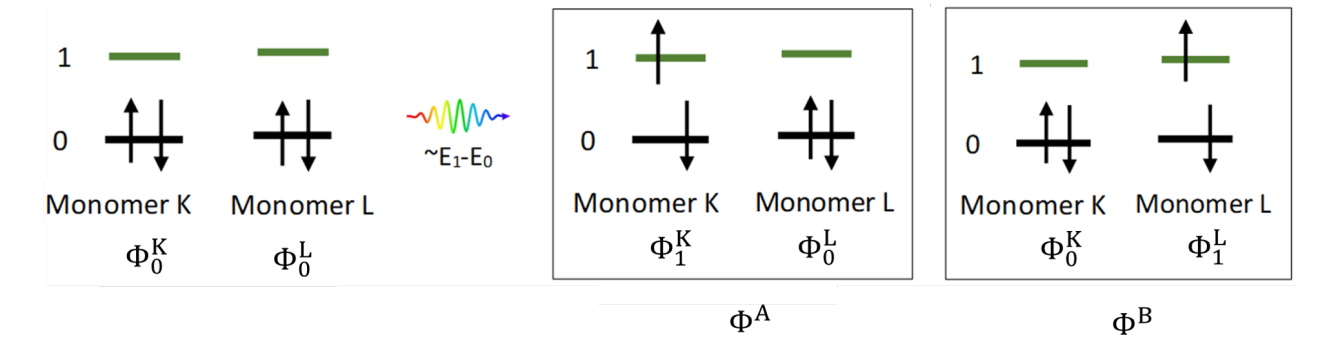
## 2.1 Theory

#### 2.1.1 Molecular Exciton Model

We consider two weakly interacting identical chromophores, K and L, where each one can be electronically excited, as shown in Scheme 1. At the limit of weak interactions we can consider the zeroth-order wavefunctions to be  $\Phi^A$  and  $\Phi^B$ , with one monomer at a time being excited while the other remains in the ground state. Considering symmetry the zeroth order wavefunction  $(\Psi^{\pm})$  describing this system can then be written as

$$\Psi^{\pm} = \frac{1}{\sqrt{2}} (\Phi^A \pm \Phi^B). \tag{1}$$

This description neglects charge transfer contributions between the two monomers and



Scheme 1: Representation of the electronic configurations describing the dimer. Indices 0 and 1 denote ground and excited state, respectively.

the overlap of their wavefunctions. In addition, the wavefunctions  $\Phi^A$ ,  $\Phi^B$  are products of the monomer wavefunctions, so the exchange term between monomers is also neglected. Finally, only the electronic wavefunctions are considered and vibrations are neglected. The

total Hamiltonian of the system consists of the Hamiltonian for each monomer plus their interaction, which introduces a coupling between them,

$$\left\langle \Psi^{\pm} \middle| \hat{H}^K + \hat{H}^L + \hat{J}^{KL} \middle| \Psi^{\pm} \right\rangle. \tag{2}$$

The interaction between monomers K and L,  $\hat{J}^{KL}$ , is given in atomic units as

$$\hat{J}^{KL} = \sum_{i}^{n_K} \sum_{j}^{n_L} \frac{1}{|r_i - r_j|} \tag{3}$$

where i and j are indices of the electrons of chromophore K and L, respectively, and  $r_i$  and  $r_j$  are their positions.  $n_K$  and  $n_L$  are the number of electrons for chromophore monomer K and L, respectively. When monomers K and L are identical in molecular structure and geometry,  $n_K$  and  $n_L$  are equal and states  $\Phi^A$  and  $\Phi^B$  are degenerate, and we can use the degenerate perturbation theory to calculate the magnitude by which the monomers perturb each other,

$$\left\langle \Psi^{\pm} \middle| \hat{J}^{KL} \middle| \Psi^{\pm} \right\rangle = \frac{1}{2} \left\langle \Phi_1^k \Phi_0^L \pm \Phi_0^k \Phi_1^L \middle| \hat{J}^{KL} \middle| \Phi_1^k \Phi_0^L \pm \Phi_0^k \Phi_1^L \right\rangle = \pm J_{KL} \tag{4}$$

As mentioned above, only the Coulombic term is included here and not the exchange interactions. Assuming the two monomers have perfectly degenerate excitations, the coupling operator has inverse dependence on the separation distance so that at separation distances where the monomers are interacting we will see energy splitting of magnitude  $2J_{KL}$ , with one energy above and one below the monomer excitation energy  $E_1$ . This splitting will die off rapidly by increasing the separation distance as the coupling term goes to zero. The exciton coupling in this case is the difference in the monomeric energy splitting divided by 2,  $J^{\Delta E}$ , which in principal will be equal in magnitude to  $J_{KL}$ . In reality, molecules are not two-level systems, and the electronic excited state will interact with other excited states, so the calculated  $J^{\Delta E}$  will deviate from the magnitude of  $J_{KL}$ .

#### 2.1.2 Modeling the Excitonic Coupling

Since we are neglecting the Dexter<sup>53</sup> exchange term arising from the indistinguishability of the electrons in the many body system wave function,<sup>54</sup> the coupling  $\pm J_{KL}$  includes only the Coulombic term. The electronic coupling can be modeled to a good approximation as the electrostatic interaction between the two monomers' electronic transition densities <sup>31,55,56</sup> as

$$J^{ETD} = \int \int \frac{\rho^{K,t}(r_K)\rho^{L,t}(r_L)}{|r_K - r_L|} dr_K dr_L$$
 (5)

where  $\rho^{K,t}$  and  $\rho^{L,t}$  are the transition densities of the chromophores K and L

$$\rho^{K,t}(r_K) = \int \Phi_0^{*K} \Phi_1^K d\tau \qquad \qquad \rho^{L,t}(r_L) = \int \Phi_0^{*L} \Phi_1^L d\tau \qquad (6)$$

where  $\tau$  denotes integration over all electrons except one in each monomer. Equation 5 is implemented in the transition density cube method  $^{27,28}$  where for each chromophore the transition density is calculated as a product of electronic ground and excited state integrated over a three-dimensional grid of finite-sized volume elements. Despite the approximations, this method offers a high-level of accuracy, especially for short-range interactions, however it can be computationally expensive.

In analogy to the classical decomposition of the electronic density into point charges localized on the atoms' nuclear centers, we can decompose the electronic transition density into atomic transition charges centered on the atomic centers, (tqs). <sup>25,36,57–59</sup> Hence, Equation 5 becomes

$$J^{tq} = \sum_{I}^{N_K} \sum_{I}^{N_L} \frac{q_I^t q_J^t}{|R_I - R_J|} \tag{7}$$

 $N_K$  and  $N_L$  are the number of atoms in each chromophore, and  $R_I$ ,  $R_J$  are the nuclear coordinates. Mulliken population analysis has been used extensively to derive the atomic transition charges from the electronic transition density matrix between ground and excited singlet state the same way we would use it to derive the classical partial charges from the

electronic density matrix of a single state. <sup>25,60,61</sup> In the Mulliken-based treatment, we use the transition density matrix between the ground and an excited state to calculate the atomic transition charges in a similar way that it is done for the electron density of an individual electronic state. <sup>25,32</sup> In this approach, electrons associated with basis functions centered on a given atom are used in calculating the partial charge of that atom, while electrons 'shared' between basis functions centered on different atoms are divided evenly between the two atoms.

Another method to derive the atomic transition charges is to determine the transition electrostatic potential (trESP) from ground to excited state. The trESP method uses the same approach as the one used to derive charges from a single state, <sup>62</sup> except that the potential is obtained from the transition density matrix between ground and excited state instead of the electronic density matrix of a single state, and it ignores the nuclear contributions to the ESP. <sup>31,33,63</sup> So, in this approach the electrostatic potential based on the transition density is calculated on a grid surrounding the molecule. Charges are obtained as best fits to reproduce the electrostatic potential. Then, one can decompose the trESP into point charges centered on the atomic centers using fitting treatments, such as MK, CHELPG, and others. Fitting the trESP using some of theses treatments is presumed to overcome the pitfalls of the Mulliken charges which mainly arise from the equal distribution of the terms involving overlaps between basis functions on different atoms.

Since the total number of electrons does not change upon electronic transitions, the sum of all atomic transition charges must be zero. The quality of the atomic transition charges is determined by their ability to reproduce the strength  $(\mu)$  and orientation of the *ab initio* transition dipole moment (esTDP) calculated by the corresponding *ab initio* method from which the transition density matrix was obtained. Of course, the *ab initio* TDP should ideally also reproduce the known experimentally determined TDP, for relevance to experiment. Similar to the permanent dipole moment, the transition dipole moment  $(\vec{\mu})$  calculated from

the atomic transition charges is

$$\vec{\mu} = \sum_{i} q_i^t \vec{r_i} \tag{8}$$

It is also important to check on the ability of the *ab initio* methods, and subsequently the tqs, to reproduce the orientation of the experimental TDP (exTDP). Consistent orientation of the tqTDP with the corresponding esTDP is crucial for a high-quality tq set.<sup>64,65</sup>

In the PDA the transition densities are approximated by the point transition dipole. <sup>45–47,54,57,66</sup> The coupling is then treated as a simple dipole-dipole interaction, given in Equation 9, such that

$$J^{PDA} = \frac{\vec{\mu}_K \cdot \vec{\mu}_L}{\vec{R}_{KL}^3} - \frac{3(\vec{\mu}_K \cdot \vec{R}_{KL})(\vec{\mu}_L \cdot \vec{R}_{KL})}{\vec{R}_{KL}^5} = \frac{\kappa \mu_K \mu_L}{R_{KL}^3}$$
(9)

where,  $\mu_K$  and  $\mu_L$  are the transition dipole moment strengths, esTDP, of monomers K and L, respectively, corresponding to the magnitude of the vectors  $\vec{\mu}_K$  and  $\vec{\mu}_L$  calculated from the corresponding *ab initio* methods.  $R_{KL}$  is the magnitude of the separation of the monomers K and L  $\vec{R}_{KL}$ .  $\kappa$  is the orientation factor which is expanded as

$$\kappa = 2\cos\theta_K\cos\theta_L + \sin\theta_K\sin\theta_L\cos\varphi \tag{10}$$

 $\theta_K$  and  $\theta_L$  are the angles between the transition dipole moments' vectors of monomers K and L, respectively, and the center-of-mass separation vector.  $\varphi$  is the twist angle between the transition dipole vectors of monomers K and L. The parameters  $R_{KL}$ ,  $\varphi$ ,  $\theta$ ,  $\theta_K$  and  $\theta_L$  are illustrated in Figure 2.

## 2.2 Computational Details

In this section, we will discuss the electronic structure methods used in this work. The Cy3 structure was optimized using density functional theory (DFT) with the B3LYP hybrid functional <sup>67</sup> and 6-31G(d) basis set; polarizable continuum model (PCM) was used to implicitly account for the solvent effect of water or methanol. This optimized monomer is then used to build the homodimer constructs. Cy3 with N-ethyl and N-propyl groups were

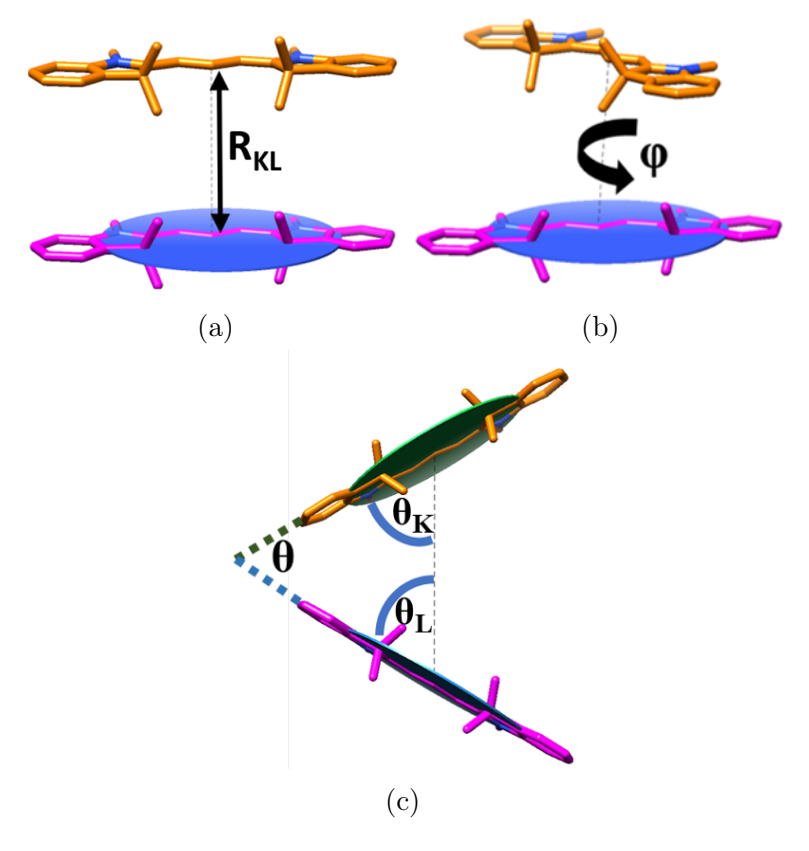


Figure 2: Definition of geometrical variables used in the systematic study on the Cy3 dimer. To construct the face-to-face homodimers, two Cy3 monomers are superimposed using their center-of-masses (COM) at the origin (0, 0, 0). (a) Dimer COM separation distance  $R_{KL}$ ; (b) twist angle  $(\varphi)$ , with  $\varphi$  equal to  $0^{\circ}$  at parallel face-to-face conformation and  $\pm 180^{\circ}$  at anti-parallel conformation; (c) tilt angle  $(\theta)$  symmetrically, with  $\theta$  equal to  $0^{\circ}$  at parallel face-to-face conformation.  $\theta_K$  and  $\theta_L$  are the angles between the transition dipole vectors of monomers K and L, respectively, and the center-of-mass separation vector.

also optimized using B3LYP/6-31G(d), as well as Parametric Method 3 (PM3),<sup>68</sup> with and without the inclusion of water or methanol solvent effects via PCM.

All the excited state calculations for the Cy3 cation monomer and the homodimer constructs were performed using several single-reference methods. We used CIS, <sup>69</sup> and TDDFT with the hybrid B3LYP functional, and long-range-corrected functionals ( $\omega$ B97, LC- $\omega$ PBE, and CAM-B3LYP). <sup>70</sup> We also tested various basis sets including split valence with polarization (Def2SVP), polarization and diffuse functions (6-31+G(d)), and Dunning's correlation-consistent triple- $\zeta$  basis sets (cc-pVTZ). The excited state energies/properties of the best

performing method were compared to results from ADC2(2). 71

The optimization of the covalently linked homodimer structure was done using B3LYP/6-31G(d) and PM3 optimization calculations in the presence and absence of counterions ( $ClO_4^-$ ) in implicit solvent (methanol) via PCM. The solvent and counterions were chosen to mimic the experimental conditions in these systems. <sup>49,50</sup> All the dimer structures were built using Chimera <sup>72</sup> version 1.14 and some structural modifications such as adding the N-alkyl groups and the bridging were done using Gaussview version 6.0. <sup>73</sup>

DFT, CIS and TDDFT calculations were performed using the Gaussian 16 package.<sup>73</sup> ADC(2) calculations on the monomer and homodimer structures were done using Q-Chem version 5.3.<sup>74</sup> and Turbomole version 6.5.,<sup>75</sup> respectively. PCM for DFT, CIS and TDDFT calculations was included using the linear-response non-equilibrium formalism, as implemented in Gaussian.<sup>76,77</sup> PCM for ADC(2) was done using the state-specific non-equilibrium formalism, as implemented in Q-Chem.<sup>78,79</sup>

Using Multiwfn version 3.7,<sup>33</sup> we extracted the transition density matrices of the different excited state calculations on the monomers (Section 3.1). Using the same package, we derived the transition atomic charges using Mulliken and trESP treatments. The CHELPG fitting scheme was used for the trESP treatment.

## 3 RESULTS AND DISCUSSION

## 3.1 Monomer properties

In this section we will discuss the calculations on the electronic structure of the singlet states,  $S_n$ , where n is the  $n^{th}$  excited state, of the Cy3 monomer.

#### 3.1.1 Excitation energies

Table 1 shows the results of energies and properties for the  $S_1$  state at vertical excitation in implicit water via PCM. The methods shown are CIS, TDDFT with four different func-

Table 1: Cy3 monomer electronic properties. Results on vertical excitations for Cy3 monomer in aqueous solvent (structure obtained from B3LYP/6-31G(d)/(PCM=Water) optimization). Excitation energies E (eV), oscillator strengths (f), strength of the transition dipole moment derived from the *ab initio* methods, esTDP (Debye), and strength of the transition dipole moment derived from atomic transition charges, tqTDP (Debye). Experimental values are:  $E^{Exp}(\pi\pi^*) = 2.25 \text{ eV}^{80-84}$  and exTDP = 12.8 Debye<sup>8,9</sup>

Method	Basis set	E $\pi\pi^*$	f	esTDP	$\operatorname{tq}$	tqTDP
CIS	Def2SVP	3.4986	1.8401	11.78	Mulliken	12.34
					${ m trESP}$	11.75
	6-31+G(d)	3.4704	1.8393	11.82	Mulliken	11.28
					${ m trESP}$	10.87
	cc- $pVTZ$	3.4828	1.8140	11.72	Mulliken	12.21
					${ m trESP}$	11.69
B3LYP	Def2SVP	2.6455	1.5163	12.29	Mulliken	12.35
					${ m trESP}$	12.25
	6 - 31 + G(d)	2.6230	1.5274	12.39	Mulliken	14.94
					trESP	14.77
	cc- $pVTZ$	2.6181	1.5079	12.32	Mulliken	12.63
					trESP	12.27
$\omega \mathrm{B}97$	Def2SVP	2.8786	1.6415	12.26	Mulliken	12.42
					trESP	12.23
	6-31+G(d)	2.8529	1.6464	12.34	Mulliken	14.17
					trESP	12.25
	cc- $pVTZ$	2.8498	1.6315	12.29	Mulliken	12.60
					trESP	12.24
$LC-\omega PBE$	Def2SVP	2.8534	1.6385	12.31	Mulliken	12.46
					trESP	12.27
	6-31+G(d)	2.8326	1.6434	12.37	Mulliken	15.05
	TIME	2 222	4 004 7	10.00	trESP	12.29
	cc- $pVTZ$	2.8285	1.6315	12.33	Mulliken	12.83
CAM DOLLAD	D focul	2 7007	1 00 10	10.00	trESP	12.29
CAM-B3LYP	Def2SVP	2.7997	1.6048	12.29	Mulliken	12.40
	C = 0.1 + O(1)	0.7765	1 (100	10.00	trESP	12.26
	6-31+G(d)	2.7765	1.6128	12.38	Mulliken	13.77
	VIDI	0.7700	1 5050	10.20	trESP	12.27
	cc- $pVTZ$	2.7728	1.5958	12.32	Mulliken	12.70
ADC(2)	Def2SVP	9 91 47	1 2001	19 99	trESP	12.27
ADC(2)		2.3147	1.3221	12.23		
	6-31+G(d)	2.2785	1.3115	12.28		

tionals, and ADC(2) which is used as a benchmark. The CIS and TDDFT methods used in this study overestimate the  $S_0 \to S_1$  transition energies of the  $\pi\pi^*$  transition responsible for the experimentally observed maximum absorption around 550 nm (2.25 eV)<sup>80–84</sup> CIS overestimates the  $\pi\pi^*$  transition energy by  $\sim 1.33$  eV, on average, as is expected from this method. <sup>85</sup> The TDDFT methods show a significantly better performance compared to CIS, with B3LYP showing the best performance with average deviation of 0.41 eV for the three different basis sets. CAM-B3LYP is the best performing long-range-corrected functional with average deviation of 0.57 eV, followed by LC- $\omega$ PBE and  $\omega$ B97 which deviate from experiment by 0.62 and 0.67 eV, respectively. These energies are still too high compared to experiment. It has been shown before that TDDFT fails to accurately predict the excited state in cyanines. <sup>86–89</sup> ADC(2), on the other hand, shows very good agreement with experiment. The deviation between ADC(2)/Def2SVP and the experimental absorption maximum is 0.06 eV, while ADC(2)/6-31+G(d) deviates by 0.02 eV.

The basis sets show small effect on the performance of all methods. We were not able to perform the ADC(2) calculations with the cc-pVTZ basis set, but based on the small basis set effect, we expect that the results will not be much different. The overall variation by basis set never exceeds 0.1 eV, and in most cases is much smaller than that.

#### 3.1.2 Transition Dipole Moment

When deriving transition charges it is crucial to check the ability of the different methods to reproduce the experimental transition dipole moment (exTDP). In addition to comparisons with experiment, where it is difficult to make straightforward comparisons, we will also use the ADC(2) values as a benchmark. The calculated values are given in Table 1, while the deviations from experiment are shown pictorially in Figure 3. The exTDP<sup>9</sup> used in the comparison is obtained from measurements on Cy3 monomer in DNA environment. The DNA environment does not have any special effect on the spectra compared to water or methanol. <sup>9,84</sup> We demonstrate this by overlaying the experimental spectra in Section SI-7.

While all methods show some deviation from exTDP, the TDDFT and ADC(2) values are very similar. This is different from what had been seen for the energies, and indicates that TDDFT can describe the transition moments better than the energies. All methods underestimate exTDP. In Figure 3, CIS shows larger deviation compared to the TDDFT functionals, which are showing close performance to each other. Within the same functional, the deviation of the calculated TDP from the exTDP consistently shows that 6-31+G(d) is somewhat better in performance followed by cc-pVTZ and Def2SVP. This indicates that addition of diffuse functions is more important than expanding the number of valence functions.

All theoretical values however are still different from exTDP, indicating that other reasons may affect the accuracy of the theoretical values. Although the environment does not seem to be significantly important there are other effects, such as vibronic effects, which can influence the comparisons we make with calculated values at vertical excitation. In order to check for these effects we calculated the TDP using LC-wPBE/Def2SVP at the excited state minimum optimized using CAM-B3LYP/6-31G(d). The value of TDP increases from 12.31 D to 12.58 D. This increase indicates that using the value at the vertical excitation is not sufficient and may contribute to our discrepancy with experiment.

It should be noted that the values of TDP are also sensitive to the formalism used for their derivation. <sup>90</sup> The oscillator strengths (f) calculated in the length, velocity and mixed gauges can differ by about 7% for the same method. We report values using the length gauge here. There are also differences if the linear response or expectation value formalism is used. When using ADC(2) we noticed that the linear response value differed from the intermediate state representation by 0.8 D. This deviation is in agreement with previous work. <sup>90</sup> Overall, the differences in the values based on the formalism are larger than the differences with experiment, so this is another source of error leading to the observed deviations from experiment.

While acknowledging that there are limitations to our comparisons with experiment we will use comparison of the vertical excitations with ADC(2) as our guide to continue. Based

on the fact that ADC(2) is not performing much better than TDDFT, despite its computational demand, we present transition charges from CIS and TDDFT for the purpose of determining the best performing method. Obtaining transition charges from ADC(2) is furthermore currently not implemented.

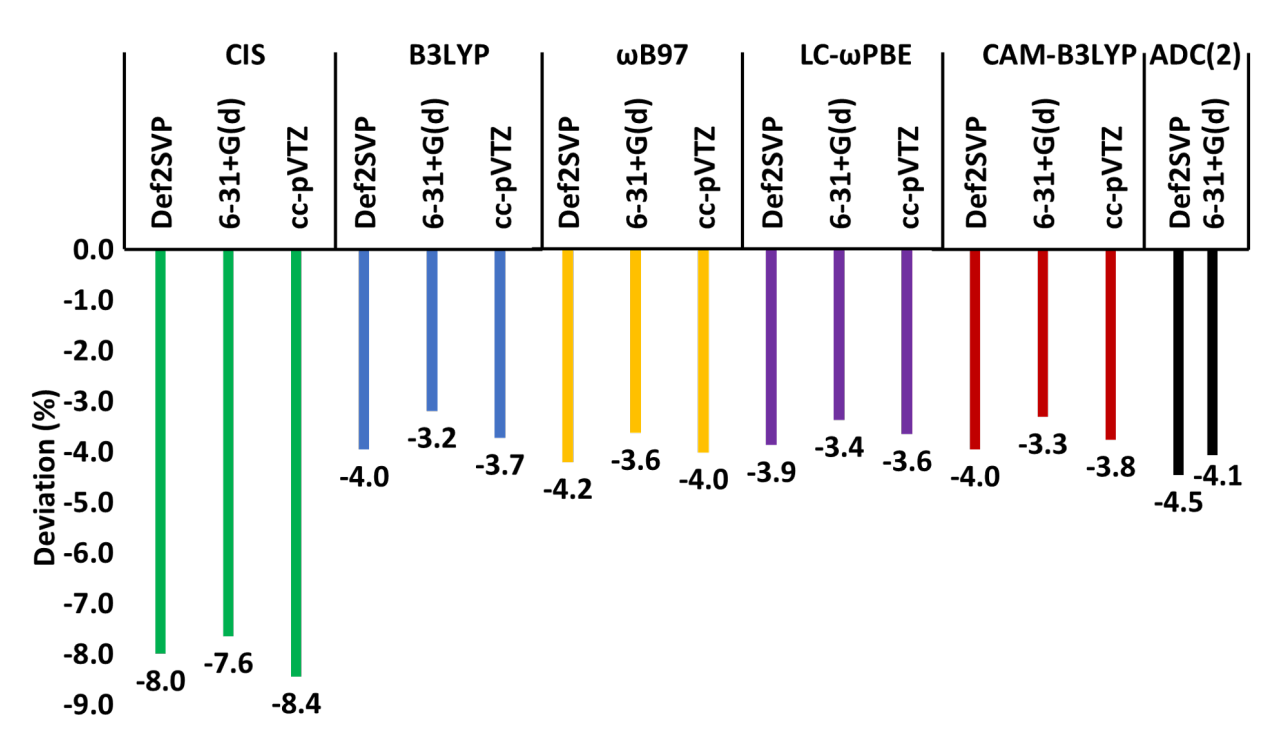


Figure 3: Deviation % of calculated monomer transition dipoles (esTDP) from the experimental transition dipole (exTDP).

#### 3.1.3 Transition Atomic Charges: Mulliken vs trESP

The transition density matrices of the  $S_0 \to S_1$  transitions are used to derive the atomic transition charges of the Cy3 monomer using the Mulliken and the trESP treatments. To better ascertain the performance of these sets of tqs, their capability to reproduce their corresponding esTDP must be determined, as shown in Figure 4 and Table 1.

The overall performance of the methods clearly shows a superiority for the trESP method over the Mulliken treatment. trESP-based tqTDPs consistently display better performance compared to the Mulliken-based tqTDPs, except for the tqs derived from CIS/6-31+G(d) which give the only case where Mulliken tqs perform better than the trESP tqs. Mulliken

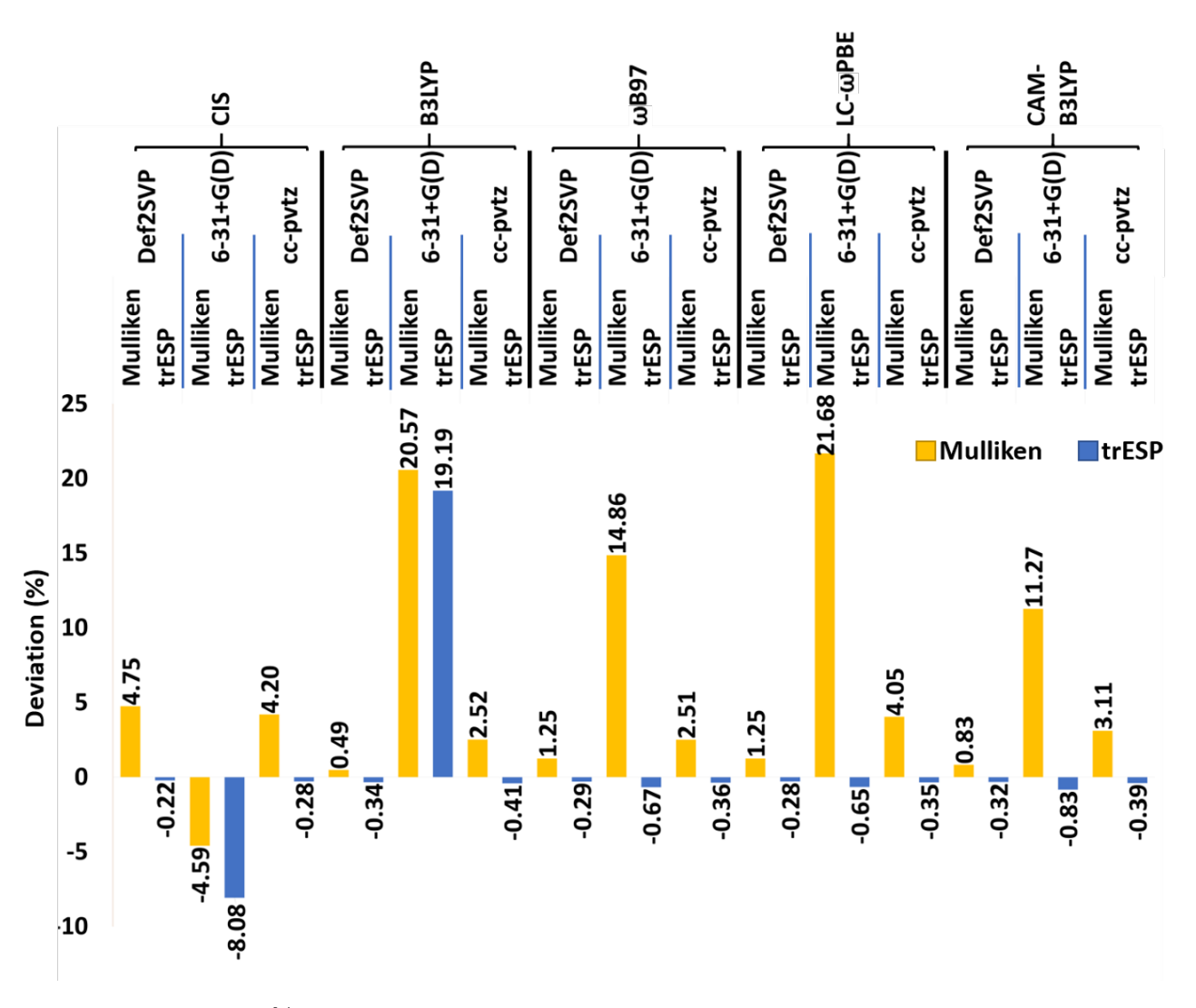


Figure 4: Deviation % of transition dipoles calculated from the atomic transition charges (tqTDP) from calculated esTDP. Mulliken and trESP charges are calculated for each method

charges also show a dependence on the basis set, with the 6-31+G(d) basis producing the largest deviations from esTDP. The errors from trESP are in general very small, except for CIS and B3LYP using the 6-31+G(d) basis set. In general, we see more dependence on the basis sets, and we find that Def2SVP is the best performing basis set followed by cc-pVTZ. Even though the diffuse orbitals produce a better esTDP, they are not very helpful in determining tqs. The superiority of the trESP charges over the Mulliken charges is expected, because of the inherent errors in the latter approach which have been discussed extensively for ground state charges. <sup>91,92</sup>

In order to decide on the best performing method, we need to consider how well the abinitio methods predict the experimental TDP (Figure 3), and how well the tqs match the esTDP for a method (Figure 4). For example, in Figure 4, even though two of the CIS trESP calculations provide the smallest deviation in Figure 4, CIS does not perform well in predicting the exTDP, as shown in Figure 3, so CIS is not a good choice. DFT-based calculations have better performance in reproducing the experimental transition dipole, as shown in Figure 3. Among them, we find the tq set derived from LC- $\omega$ PBE/Def2SVP/trESP to be the best choice, since this approach satisfies all the transition atomic charges quality conditions. The esTDP deviation from the experimental exTDP is -3.9\% and the deviation of the tqTDP from the esTDP is -0.28%. Also, the set's tqTDP orientation aligns well with the esTDP. The  $\omega$ B97/Def2SVP/trESP and CAM-B3LYP/Def2SVP/trESP are the second and third best performing to sets, respectively. Therefore, in the following sections, we will be testing the quality of the LC- $\omega$ PBE/Def2SVP/trESP by monitoring their performance in calculating the excitonic coupling between artificial and experimental Cy3 homodimer constructs. The structure of the monomer and the LC- $\omega$ PBE/Def2SVP/trESP charges can be found in Table S2. Plots of the tq sets obtained from the Mulliken and trESP treatments and more performance analysis can be found in the Supporting Information, Section SI-2.

#### 3.1.4 Effect of the N-alkyl groups on the monomer's electronic properties

When Cy3 is used to label systems like proteins and DNA, it is usually attached to these systems via saturated aliphatic hydrocarbon linkers (N-alkyl groups). <sup>6,8,9,12,93</sup> If the N-alkyl groups affect the electronic properties of the monomer, then one must account for them while deriving the atomic transition charges of the monomer. To investigate the effect of the N-alkyl groups on the monomer, we extended our electronic structure calculations on the Cy3 with N-methyl groups to N-ethyl and N-propyl groups, as shown in Figure 5.

The structures were optimized using B3LYP/6-31G(d) and PM3 in gas phase as well as implicit solvent (water or methanol). The same set of excited state methods and basis

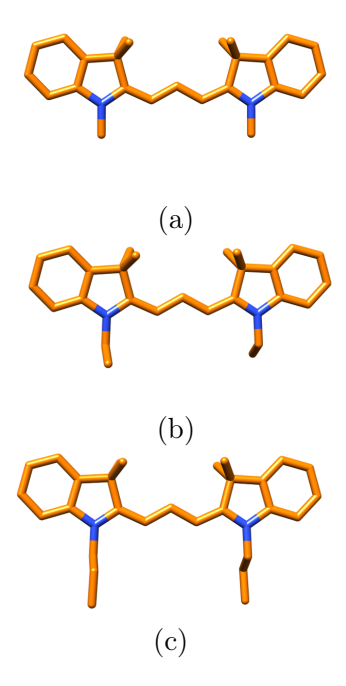


Figure 5: Representation of the Cy3 monomer with N-methyl groups (a), N-ethyl groups (b), N-propyl groups (c).

sets were used as before to calculate the monomers' excitation energies  $(S_1)$  and their corresponding transition dipole moments, esTDP. Results for the method and basis set that produced the highest quality atomic transition charges set (LC- $\omega$ PBE/Def2SVP) are shown in Figure 6.

As shown in Figure 6, there is little to no effect from the different N-alkyl groups on the  $S_1$  energies and the transition dipole moments of the Cy3 monomer. This suggests that including N-alkyl groups beyond N-methyl in the *ab initio* optimizations and the excited state calculations might not be necessary, especially if expensive methods are used. The effect of the geometry on these properties is also examined by comparing the results obtained from B3LYP optimized geometries to those from PM3 geometries. The optimization method has a significant effect on the monomers' structures, which can in turn influence the magnitude of the calculated TDP. The main observation is that the B3LYP/6-31G(d) optimizations result in structures with longer axis compared to those optimized using PM3, as shown in Figure S6 and Table S6. For example, the RMSD between the N-methyl B3LYP/water structure (long-axis measuring 14.18 Å) and N-methyl PM3/water structure (long-axis measuring 13.71 Å) is

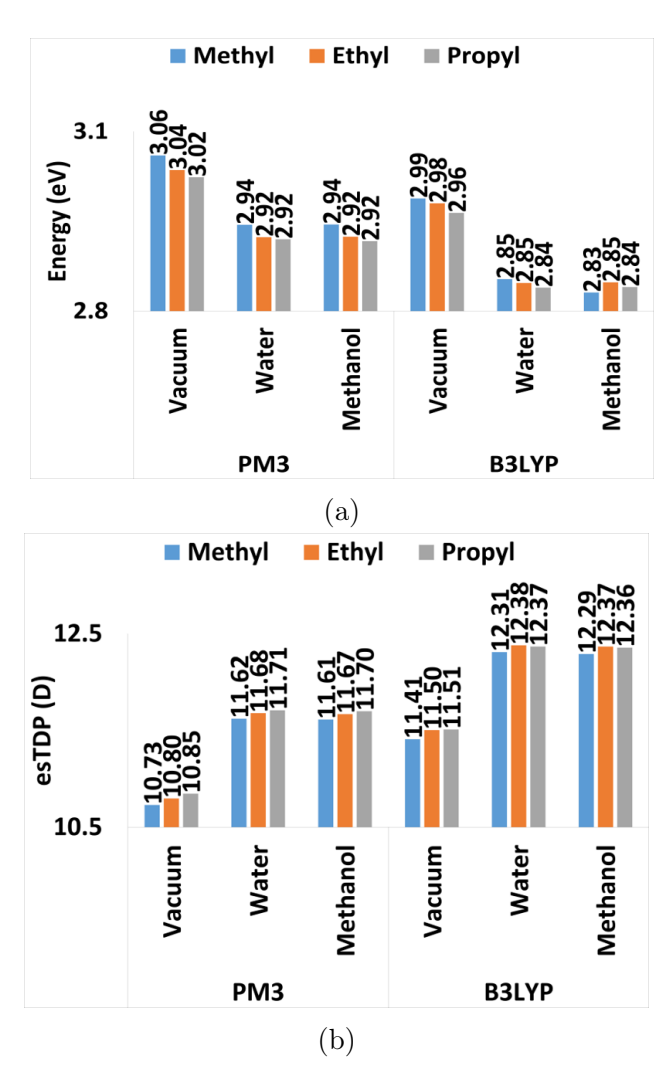


Figure 6: Excited state calculations (LC- $\omega$ PBE/Def2SVP) done in vacuum and implicit water and methanol on the monomer with N-methyl (blue), N-ethyl (orange), and N-propyl (grey) groups. Monomers' structures obtained from PM3/PCM=water and B3LYP/6-31G(d)/PCM=water optimizations. (a) Vertical  $S_1$  excitation energy (b)  $S_1$  transition dipole moment (esTDP).

0.548 Å. It is easy to see a correlation between the length of the long axis and the magnitude of the *ab initio* transition dipole (esTDP); for example, the structures obtained from the B3LYP/water optimizations resulted in esTDPs of  $\sim$ 0.7 Debye larger magnitude compared to the PM3/water optimized structures. On the other hand, the effect of the geometries on the  $S_1$  energies is less than 0.1 eV.

When comparing the excitation energies obtained in gas phase and a solvent of water or methanol, we see that water and methanol give identical results, while the gas phase results differ by a small amount (about 0.1 eV). These results agree with experimental absorption spectra which are very similar in water and methanol.<sup>50,84</sup> The effect of solvent is more pronounced on the esTDP (about 1 D between gas phase and solution) and subsequently the quality of the transition charges. The solvents water and methanol give practically identical results for esTDP, as well. This suggests that solvent effects should be accounted for when calculating the transition dipoles (esTDP) and their transition charges (tqs), although the exact nature of a polar solvent is less important.

The behavior of transition energies and the transition dipole magnitudes obtained from all the different methods included in this part are consistent with what we have seen from the  $LC-\omega PBE/Def2SVP$ . The results obtained from the rest of the excited state calculations can be found in SI-6.2 and SI-6.3. Overall, these results suggest that including N-alkyl groups larger than the N-methyl is not important when obtaining the tqs, but the environment and geometries are.

## 3.2 Systematic study on the Cy3 homodimer

In this section, the performance of (LC- $\omega$ PBE/Def2SVP/PCM=water) tqs is evaluated by calculating the excitonic coupling as a function of distance, and comparing it to the coupling obtained from *ab initio* calculations of the dimer. The PDA coupling is also calculated for comparison.

### 3.2.1 Coupling as a function of the center-of-mass, COM, separation $(R_{KL})$

We will first examine the effect of varying the separation distance  $(R_{KL})$ , as defined in Figure 2a, on the excitonic coupling of Cy3 homodimer. Choosing the anti-parallel conformation  $(\varphi=180^{\circ})$  to study the coupling behavior as a function of  $R_{KL}$  enables us to sample separation distances as small as 3 Å which are not physically possible in the parallel orientation  $(\varphi=0^{\circ})$  due to the monomers' atoms overlap. The parallel orientations at larger separation distances are included in the following part where we study the effect of varying the twist angle  $(\varphi)$ . The couplings obtained from tqs (LC- $\omega$ PBE/Def2SVP/trESP), PDA, or supermolecule

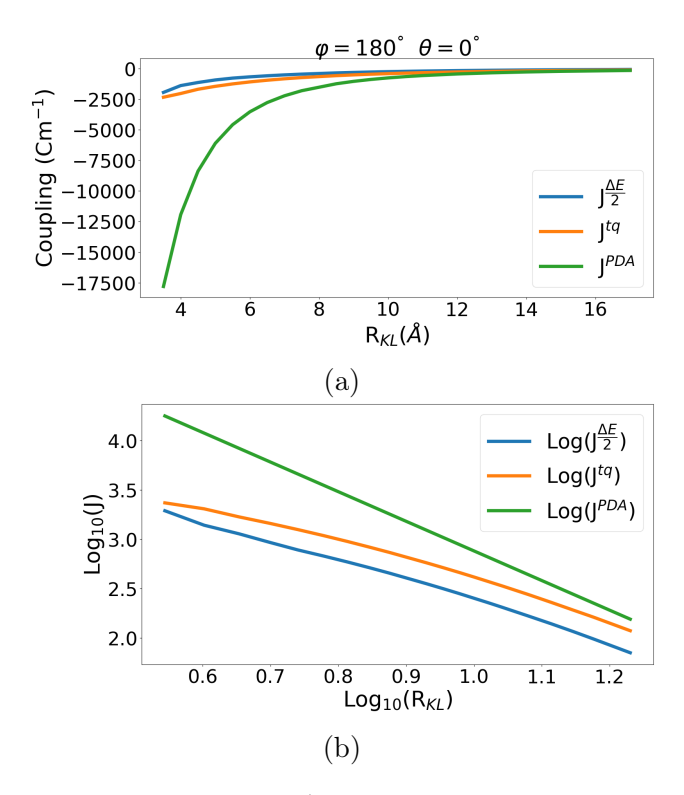


Figure 7: Coupling based on *ab initio*  $(J^{\frac{\Delta E}{2}})$ , tqs  $(J^{tq})$ , and PDA  $(J^{PDA})$  as a function of the center-of-mass separation COM.  $\varphi = 180^{\circ}, \theta = 0^{\circ}$  (a) logarithmic scale (b). The LC- $\omega$ PBE/Def2SVP/PCM=Water) method is used, and the charges are obtained from trESP.

excitation calculations (LC- $\omega$ PBE/Def2SVP/PCM=Water) are shown in Figure 7. The tqs overestimate the supermolecule *ab initio* couplings over all the separation distances. At very small separation distances  $\sim 3-7.5\text{Å}$ , the ratio of the  $J^{tq}$  to the  $J^{\frac{\Delta E}{2}}$  is around 1.6. The ratio at intermediate ranges and at separations comparable to the monomer's long axis (14)

Å) is around 1.5. At larger separation distance, 17 Å, the ratio goes down to 1.2. The drop in the  $J^{tq}$  to the  $J^{\frac{\Delta E}{2}}$  ratio at larger separation ratio indicates that the Coulombic coupling is dominating the electronic interactions. The close ratios at the small and intermediate separations suggest that the tq performance in these ranges is consistent and reliable.

The  $J^{PDA}$  is much larger than both  $J^{\frac{\Delta E}{2}}$  and  $J^{tq}$ , and the discrepancy increases rapidly as the distance  $(R_{KL})$  decreases. As expected, the PDA breaks down at separation distances comparable to and lower than the dimensions of the monomer's long axis. By increasing the separation distances, the PDA couplings show a very fast exponential drop in the couplings' magnitude and their performance become comparable to the  $J^{\frac{\Delta E}{2}}$  and  $J^{tq}$  at  $R_{KL}\approx 12$  Å. The PDA at the large separation distance is quite close to the *ab initio* calculations with deviation of 110 cm<sup>-1</sup> at 15 Å and 57 cm<sup>-1</sup> at 17 Å. At close separation distance of  $\sim 3$ Å, the  $J^{PDA}$  to  $J^{tq}$  ratio is around 7, and it decreases to 3 at  $R_{KL}=7$ Å. At intermediate separation distances up to  $\sim 13$ Å, the ratio goes down to around 1.6. In the weak coupling regime the  $J^{PDA}/J^{tq}$  is 1.31. This performance shows that using PDA couplings at large separation distances can reproduce the *ab initio* supermolecule coupling with reasonable accuracy and low cost, but it should not be used at smaller distances.

The plots of  $\log(J)$  against  $\log(R_{KL})$  in Figure 7b display linearity with slopes pointing to the exponential dependence of the excitonic couplings on the separation distance. The PDA couplings slope is -3 indicating an inverse cubic dependence on the distance,  $R_{KL}^{-3}$ , while the slopes of the transition charges and *ab initio* couplings are -1.9 and -2.0, respectively.

The results here highlight the importance of avoiding using the PDA model to calculate the excitonic coupling between large monomers, like Cy3, especially if it is certain that the aggregate units are in close proximity to each other. Although the coupling from the tqs overestimate the *ab initio* couplings, their response to changes in the separation distance is consistent with the *ab initio* calculation's behavior, which makes it a better choice than PDA for modeling the excitonic couplings at small and moderate separation distances.

#### 3.2.2 Coupling as a function of the twist $(\varphi)$ and tilt $(\theta)$ angles

In this part the effect of the relative orientation on the excitonic coupling behavior will be explored. This is done via testing the dependence of the coupling on the twist  $\varphi$  and tilt  $\theta$  angles, as defined in Figures 2b and 2c, respectively. Figure 8a shows the variation of coupling as a function of  $\varphi$  for two different values of  $R_{KL}$ . As one would expect, the maximum magnitude of coupling is for parallel and antiparallel orientations, at  $\varphi = 0^{\circ}$  and  $+180^{\circ}$ , respectively. The coupling at the two orientations has the same magnitude but opposite sign.

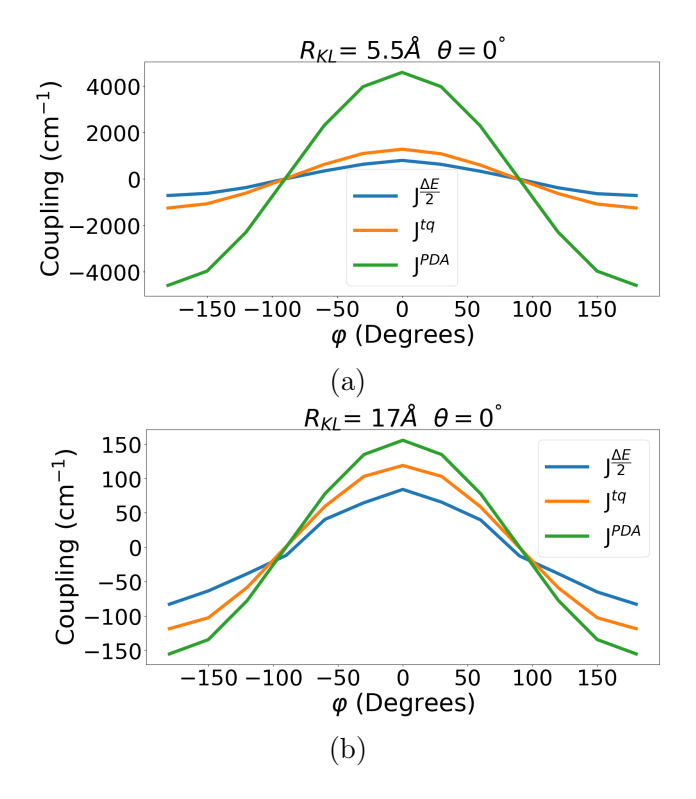


Figure 8:  $J^{\frac{\Delta E}{2}}$ ,  $J^{tq}$ , and  $J^{PDA}$  as a function of the twist angle at  $\theta = 0^{\circ}$  (a)  $R_{KL} = 5.5$  Å, (b)  $R_{KL} = 17$  Å. The LC- $\omega$ PBE/Def2SVP/PCM=Water) method is used, and the charges are obtained from trESP.

The comparison between the different methods to obtain the coupling is similar here as when varying  $R_{KL}$ . At the short distance the PDA overestimates the couplings calculated from the tqs and the *ab initio* couplings. The ratio of the  $J^{tq}$  to  $J^{\frac{\Delta E}{2}}$  is, on average, 1.6, while the PDA overestimates the  $J^{\frac{\Delta E}{2}}$  and  $J^{tq}$  with an average ratio of 5.8 and 3.7, respectively.

At this separation distance, it is clear that the PDA is unreliable, especially at twist angles close to the parallel and antiparallel orientations. There is a small region however around  $\varphi = 90^{\circ}$  that PDA is not as different as the other couplings, as they all approach zero. When we vary  $\varphi$  at larger separation distance, as shown in Figure 8b, the three methods show closer performances. The ratio of the  $J^{tq}$ s to  $J^{\frac{\Delta E}{2}}s$  is, on average, 1.7, while the PDA overestimates the  $J^{\frac{\Delta E}{2}}s$  and  $J^{tq}s$  with an average ratio of 2.2 and 1.3, respectively. The consistent performance between the tqs method and the *ab initio* calculation in the short and long distance ranges sheds more light on its superiority in describing the coupling. Since the  $\varphi$  angle is showing large contribution to the coupling, the coupling dependence on the twist angle at other separation distances spanning the small and medium coupling distances was studied, and the results are shown in Figure S4. It was found that the tq performance relative to the *ab initio* is consistent when  $\varphi$  at different separation distances is varied.

Varying the tilt angle ( $\theta$ ) symmetrically at  $R_{KL}=5.5$  Å, as described in Figure 2c, is limited by the atoms superimposing due to the close proximity of the monomers.  $\theta$  was varied between  $+25^{\circ}$  and  $-25^{\circ}$  starting from the antiparallel conformation which allowed sampling of more space. Varying  $\theta$  at this separation distance showed small to negligible effects on the coupling, as shown in Figure 9a. This recommends that the tilt angle does not have a large contribution at small separation distances. At  $R_{KL}=17$  Å, the larger separation distances allowed the sampling of the whole space by varying  $\theta$  between  $+90^{\circ}$  deg and  $-90^{\circ}$ . Compared to smaller separation distances, tq and PDA are showing coupling with closer performance, especially at large tilt angles (Figure 9b). Interestingly, the magnitude of the coupling increases as  $\theta$  moves away from  $0^{\circ}$ , and all methods are able to predict qualitatively correct behavior. The dependence of the coupling on  $\theta$  is, in general, smaller on the separation or twist angle parameters.

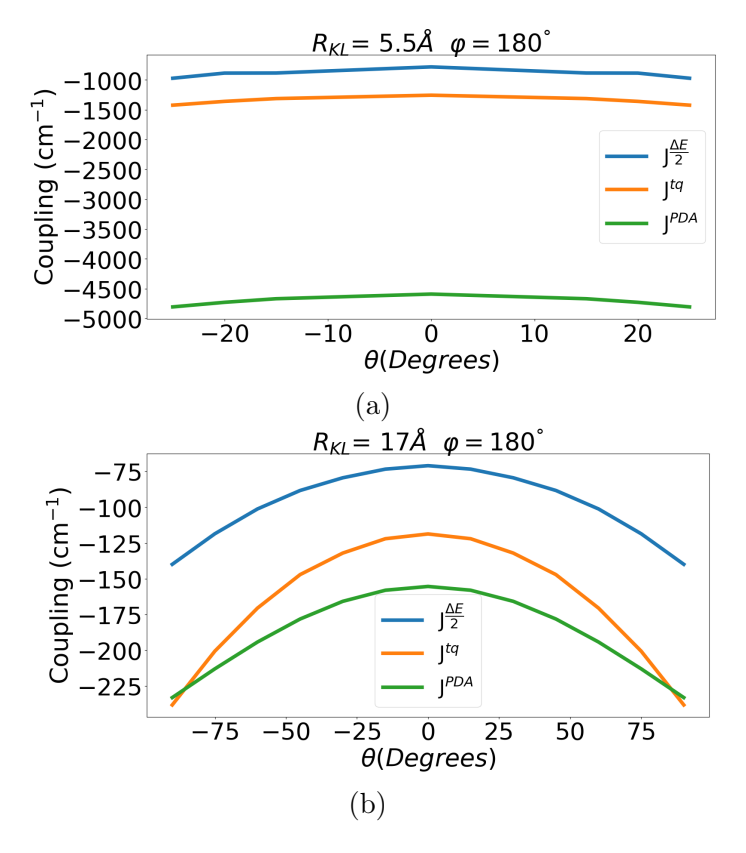


Figure 9:  $J^{\frac{\Delta E}{2}}$ ,  $J^{tq}$ , and  $J^{PDA}$  upon varying theta symmetrically at  $\varphi = 180^{\circ}$  (a)  $R_{KL} = 5.5$  Å, (b)  $R_{KL} = 17$  Å. The LC- $\omega$ PBE/Def2SVP/PCM=Water) method is used, and the charges are obtained from trESP.

## 3.3 Comparison with experimental data

After exploring the behavior of the  $J^{\frac{\Delta E}{2}}$ ,  $J^{tq}$ , and  $J^{PDA}$  as a function of the relative orientation, the ability of the chosen set of charges, LC- $\omega$ PBE/Def2SVP/trESP, to predict the excitonic coupling in a simple Cy3 homodimer that has been studied experimentally was tested. The system is shown in Figure 10.

There are two combined experimental/theoretical studies that used this system,  $^{49,50}$  and our results can be compared to the coupling obtained from those. Using a joint experimental and theoretical study, Halpin  $et\ al.^{49}$  have reported the total electronic and vibrational coupling of a biscyanine homodimer. Halpin  $et\ al.$  studied the system experimentally in methanol. They used PM3 and MM+ optimizations to get the homodimer geometry and to extract the parameters needed for the theoretical calculations. The optimization gave

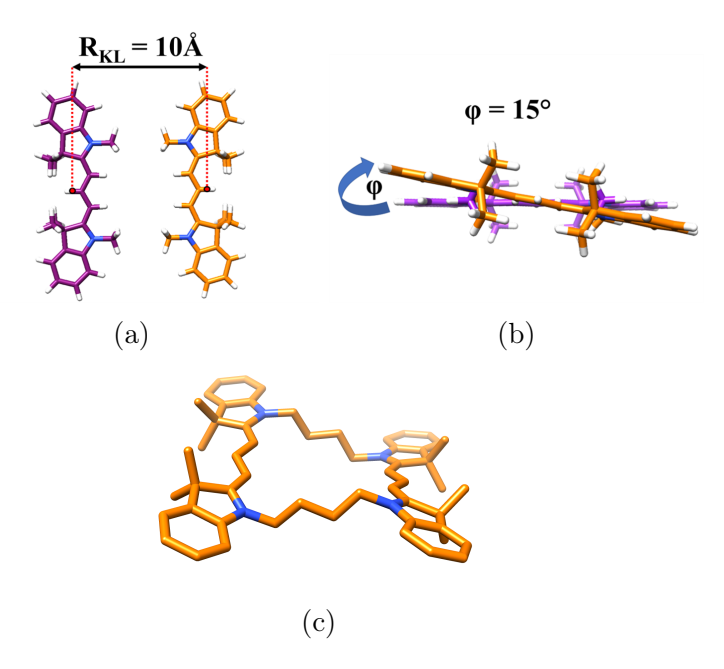


Figure 10: (a,b) Construct of artificial Cy3 dimer as reported by Halpin *et al.*.<sup>49</sup> and Duan *et al.*;<sup>50</sup> (a) COM separation distance ( $R_{KL} = 10\text{Å}$ ) (b) Side view showing twist angle ( $\varphi = 15^{\circ}$ ). (c) Structure of the artificial homodimer construct obtained from B3LYP/6-31G(d) optimization. Optimization details and results are in Section 3.3 and Table 2.

a homodimer with subunits separation distance and relative angular orientation of 10 Å and 15°, respectively. Their PM3 (ZINDO/S) semi-empirical calculations on the parent monomer gave transition dipole strength of 13 D. Using these parameters and the point-dipole approximation, they calculated the electronic coupling  $J^{PDA}$  to be 820 cm<sup>-1</sup>. They could reproduce the monomer and dimer linear absorption spectrum using the Holstein Hamiltonian vibronic exciton model and an excitonic coupling strength of 800 cm<sup>-1</sup>. Duan et al. <sup>50</sup> studied the same biscyanine construct experimentally in methanol. In their case, the best fit to the measured absorption spectrum of the homodimer was obtained for a coupling value of 870 cm<sup>-1</sup>. Further details of the Halpin et al. and Duan et al. geometry optimizations, excited state calculations, and parameters definitions can be found in the original publications. <sup>49,50</sup>

The study so far has been done using water as solvent because this is how Cy3 is used in several experiments. 80–84 However, since the Halpin *et al.* 49 and Duan *et al.* 50 experiments were done in methanol we report results in implicit solvent of methanol in this section.

Table 2: Couplings and geometries of the artificial Cy3 homodimer system. Couplings (in  $cm^{-1}$ ) calculated using the point-dipole approximation  $J^{PDA}$ , atomic transition charges  $J^{tq}$ , and ab initio methods  $J^{\frac{\Delta E}{2}}$ . The latter is calculated with (w/l) and without (wo/l) linkers. The COM separation distance  $(R_{KL})$  is in Å. The angles  $\theta$ ,  $\theta_K$ ,  $\theta_L$ , and  $\varphi$  are in degrees. All the geometrical parameters are as defined in Figure 2. The magnitude of the transition dipole transition dipole,  $\mu$ , is in Debye. Experimental values are:  $J^{Exp} = 800^{49}$  and  $870.^{50}$ 

	Halpin System	B3LYP	PM3	B3LYP $(ClO_4^-)$	$PM3 (ClO_4^-)$
$J^{tq}$	667	877	879	822	845
$J^{rac{\Delta E}{2}}$ (wo/l)/LC- $\omega$ PBE	398	537	542	560	504
$J^{rac{\Delta E}{2}}$ (wo/l)/ADC(2)	448	594	583	603	534
$J^{rac{\Delta E}{2}}$ (w/l)/LC- $\omega$ PBE		666	640	674	630
$J^{rac{\Delta E}{2}} \; ( ext{w/l})/ ext{ADC}(2)$		730	670	735	661
$J^{PDA}$	735	1132	1112	1016	1227
$R_{KL}$	10	8.56	8.65	8.98	8.13
arphi	15	21.59	19.36	15.30	29.96
heta	0	4.73	2.57	5.25	2.30
$ heta_K$	90	87.64	88.72	87.84	90.59
$ heta_L$	90	87.62	88.71	86.91	91.71

The results/couplings are not affected by the choice of water or methanol as solvent. The comparisons are shown in SI-4.1. Initially, we used the geometrical information obtained by the two previous studies to build the supermolecule dimer system, as shown in Figure 10 (a,b). The system was built using our Cy3 monomer geometry optimized at B3LYP/6-31G(d)/(PCM=Methanol).  $J^{\frac{\Delta E}{2}}$ ,  $J^{tq}$  and  $J^{PDA}$  were calculated using this structure, the results are tabulated in Table 2 in the column with the label Halpin System. Using  $\mu=12.29$  D, we calculated  $J^{PDA}=735$  cm<sup>-1</sup>. It should be noted that this is smaller than the value obtained by Halpin  $et~al.^{49}$  and Duan  $et~al.^{50}$  because that study used a larger TDP magnitude of 13 D. The excitation energies of the supermolecule construct (two monomers separated by 10 Å and twist of 15°) were calculated using LC- $\omega$ PBE/Def2SVP/(PCM=Methanol), and predicted the excitonic coupling  $J^{\frac{\Delta E}{2}}$  to be 398 cm<sup>-1</sup>. The calculated ab~initio and transition atomic charges couplings of this structure underestimate the experimental couplings reported by Halpin et~al. by 50% and 16.6 %, and of that reported by Duan et~al. by 54% and 23%, respectively.

In addition to using the reported geometry, the system was also optimized at a higher level of theory to determine how sensitive the coupling is with the geometry. Unless otherwise specified, all the results of this part are listed in Table 2. All the excited state calculations are done using LC- $\omega$ PBE/Def2SVP in methanol via PCM.  $J^{tq}$ s are calculated using LC- $\omega PBE/Def2SVP/trESP/(PCM=Methanol)$ . Optimizing the system using B3LYP/6-31G(d) in implicit solvent (PCM=Methanol) produced the structure shown in Figure 10c, with  $R_{KL}$ = 8.56 Å and  $\varphi$ = 21.59°. The values obtained are different from the previously reported ones. Using this structure, we calculated the  $J^{\frac{\Delta E}{2}}$  (without linkers)= 537 cm<sup>-1</sup> and  $J^{\frac{\Delta E}{2}}$ (with linkers) =  $666 \text{ cm}^{-1}$ . ADC(2) calculations were also performed for the homodimer structures with and without linkers. The couplings  $(J^{\frac{\Delta E}{2}})$  obtained from ADC(2) compare better to the experimental values and are higher than those obtained from LC- $\omega$ PBE by an average of 45 cm<sup>-1</sup>. Despite the improvement, ADC(2) underestimated the experimental couplings by  $\sim 67~cm^{-1}$ . For example,  $J^{\frac{\Delta E}{2}}$  obtained from the ADC(2) calculation on the B3LYP optimized structure (with linkers) deviates from the experimental value reported by Halpin et al. by 9\%, while the coupling from LC- $\omega$ PBE on the same structure deviates by 17%.

Although the *ab initio* calculations underestimate the experimental excitonic coupling, these results are a significant improvement compared to the geometry predicted by Halpin *et al.* and Duan *et al.*, especially with the inclusion of the linkers. A very important point here is the large effect of the linkers on the *ab initio* coupling. This is in contrast with what we found in Section 3.1 where the linkers do not affect the properties of the monomer. The effect on the dimer indicates that some additional through-bonding coupling is playing a role in the overall coupling. This cannot be produced by any of the other methods used in this study based on monomer properties. On the other hand, the *ab initio* coupling is still not in perfect agreement with experiment. The inability of the *ab initio* methods to capture the excitonic coupling in high-accuracy suggests the inclusion of the other states in the overall coupling. In the *ab initio* calculations all states are incorporated and can mix.

In the excitonic model, on the other hand, we are only using a two level system. Mixing with the other states will result in a deviation of this simple model. It is also possible that higher level quantum mechanical methods and larger basis sets could have an effect. Such methods however are very expensive for the dimer system, and they do not fit within our scope of searching for a cost-effective approach to generate the atomic transition charges.

Using tqs, the excitonic coupling for the B3LYP geometry was calculated to be  $J^{tq}$ = 877 cm<sup>-1</sup> while the point-dipole model gives  $J^{PDA}$ = 1132 cm<sup>-1</sup>. The coupling produced by tqs is almost identical to the experimental coupling by Duan *et al.*, while it overestimates the Halpin *et al.* coupling by 9.6 %.

To check the effect of the optimization method, the system was optimized using PM3 in methanol via PCM. The optimization using this semi-empirical method showed negligible effect on the relative orientation of the two Cy3s cations, and as a result the calculated couplings, as shown in Table 2, are also very similar. To account for the counterions used by Duan et al.,  $^{50}$  the dimer was also optimized in the presence of two  $ClO_4^-$  ions using implicit solvent (PCM=Methanol) at both B3LYP/6-31G(d) and PM3 levels. The counterions had a somewhat more important effect, and they showed a different effect at the B3LYP level compared to PM3. At the B3LYP level, the monomers were comparatively farther apart and more parallel, while at the PM3 level they were closer and less parallel. These changes lead to smaller couplings at the PM3 level, while the couplings at the B3LYP geometries were less consistent. Obviously, the effect of the counterions seems to be important and very sensitive to the method used for optimizations. Our results indicate that more work is needed to clearly understand these effects. Further investigation of the effect of the ab initio methods and basis sets on the  $J^{\Delta E}$ ,  $J^{tq}$ , and  $J^{PDA}$  of the homodimer is reported in Section SI-5.

Overall, given the difference between the two experimental values, the coupling predicted using tqs is very accurate. On the other hand, neither the PDA nor the *ab initio* couplings reproduce the experimental values. As expected, PDA overestimates the coupling while the

ab initio splitting underestimates it. The PDA value reported by Halpin et al.<sup>49</sup> and Duan et al.<sup>50</sup> are different from the results of this study and closer to the experimentally fitted value. According to this study, this appears to be because of a fortuitous cancellation of errors. In their work, these two groups had used a very long  $R_{KL}$ , which cancelled the effect of overestimating the coupling by PDA.

#### 3.4 Conclusions

Despite the great advancement in computational capabilities, studying the excitonic coupling in big systems using a high-level quantum mechanical method is often still computationally impractical. Modeling the excitonic coupling using atomic transition charges and their electrostatic coupling is a very convenient approach because of its high-accuracy when overlap and charge transfer are not important. Obtaining high-quality atomic transition charges needs a careful treatment. Proper investigation of the ability of the quantum mechanical methods to get the transition dipole moment, its magnitude and orientation, is necessary. The transition charges should be able to reproduce the corresponding *ab initio* transition dipole's magnitude and orientation.

In this paper, atomic transition charges that can, to a good accuracy, be used to model the excitonic interactions of the widely-used cyanine dye Cy3 were obtained. Several quantum mechanical methods and basis sets were tested in their ability to reproduce the exTDP. Within the limits of this study, the TDDFT method with various functionals showed reasonable and comparable ability to calculate the exTDP. The available options to derive the atomic transition charges from the corresponding TDP were examined, and found a superior performance from the transition density electrostatic potential approach compared to the Mulliken approach. Our analysis showed that the charges obtained from the LC- $\omega$ PBE/Def2SVP/trESP calculations have the highest quality and they should be a reliable option to model the Cy3 excitonic coupling. This was confirmed by calculating the coupling for an experimentally well-studied bis-indocarbocyanine dimer. The charges predicted

the coupling with high-accuracy. The atomic transition charges developed in the current study can, in principle, provide an important approach for the elucidation of bio-molecular structure in studies that utilize Cy3 labels as exciton-coupled chromophore probes.

This study also compared the excitonic couplings obtained from the atomic transition charges  $(J^{tq})$  with those obtained from the *ab initio* coupling  $(J^{\frac{\Delta E}{2}})$  and the PDA model  $(J^{PDA})$ . The results confirmed that the PDA model should be avoided to model the Cy3 chromophore excitonic coupling. It was also found that the inclusion of the N-ethyl and N-propyl groups to the Cy3 monomer had negligible effects on its  $S_1$  excitation energies and the *ab initio* transition dipoles. A prominent effect from the optimization method choice on the monomer's electronic properties was seen, and a reasonable level of theory was shown to be advisable. Finally, it was found that the solvent might have a big effect on the magnitude of the *ab initio* transition dipoles, and it must be accounted for while deriving the atomic transition charges.

## Acknowledgement

S.M. and M.I.S. acknowledge funding from the National Science Foundation, grant number CHE-1800171. A.H.M. acknowledges funding from NIH General Medical Sciences, GM-15792. This research includes calculations carried out on HPC resources supported in part by the National Science Foundation through major research instrumentation grant number 1625061 and by the US Army Research Laboratory under contract number W911NF-16-2-0189. We also thank the current and former members of the Spano Lab at Temple University, namely Mohammad Balooch, April Olson, David Bialas, and Xin Chang, for the useful conversations and helping introducing and guiding through some computational packages used in this study.

## Supporting Information Available

Supplementary material for this article is available online. Coordinates of certain monomer and biscyanine systems are introduced, along with the tq sets that displayed high-quality performance. Comparisons between the performance of the tq sets obtained in implicit solvent (water or methanol) are made. Coupling as a function of the twist angle at different separation distances is discussed. Lastly, the effects of the optimization methods, environment, N-alkyl groups, excited state methods, and basis sets dependence on monomer's ground state structure,  $S_1$  transition energies, and  $S_1$  esTDP are compared.

## Acronyms

 $J^{\frac{\Delta E}{2}}$  excitonic coupling from ab initio calculations.

 $J^{tq}$  excitonic coupling from transition charges.

 $\hat{J}^{KL}$  excitonic coupling operator.

 $\omega$ B97 Long-ranged corrected hybrid density functional. Becke.

 ${\cal J}^{PDA}$  excitonic coupling from point-dipole approximation.

6-31+G(d) polarization and diffuse basis set.

ADC(2) algebraic diagrammatic construction through second order.

**B3LYP** Becke 3-Parameter (Exchange), Lee, Yang and Parr (correlation; density functional theory).

**CAM-B3LYP** Coulomb-Attenuating Method-Becke 3-Parameter (Exchange), Lee, Yang and Parr (correlation; density functional theory).

**cc-pVTZ** Dunning's correlation-consistent polarizable triple- $\zeta$  basis set.

CHELP charges from electrostatic Potential.

CHELPG charges from electrostatic Potential, grid method.

CIS configuration interaction singles.

**COM** center-of-mass separation.

**Def2SVP** split valence with double- $\zeta$  polarization.

**EDM** extended-dipole model.

ESP electrostatic potential.

esTDP ab initio/electronic-structure transition dipole.

exTDP experimental transition dipole.

**f** oscillator strength.

FRET Förster Resonance Energy Transfer.

 $LC-\omega PBE$  Long-ranged corrected hybrid density functional. Perdew, Burke, and Ernzerhof.

MK merz-singh-kollman.

PCM Polarizable Continuum model.

**PDA** point-dipole approximation.

PM3 parametric method 3.

**RESP** restrained electrostatic potential.

TDDFT time-dependent density functional theory.

**TDP** transition dipole.

tqTDP transition charges transition dipole.

tresp transition electrostatic potential.

## References

- (1) Levitus, M.; Ranjit, S. Cyanine dyes in biophysical research: the photophysics of polymethine fluorescent dyes in biomolecular environments. Q. Rev. Biophys 2011, 44, 123.
- (2) Mishra, A.; Behera, R. K.; Behera, P. K.; Mishra, B. K.; Behera, G. B. Cyanines during the 1990s: a review. *J. Chem. Rev.* **2000**, *100*, 1973–2012.
- (3) Lee, W.; Jose, D.; Phelps, C.; Marcus, A. H.; von Hippel, P. H. A single-molecule view of the assembly pathway, subunit stoichiometry, and unwinding activity of the bacterio-phage T4 primosome (helicase–primase) complex. *Biochemistry* **2013**, *52*, 3157–3170.
- (4) Armitage, B. A. Cyanine dye-nucleic acid interactions, Heterocyclic Polymethine Dyes; Springer, 2008; pp 11–29.
- (5) Lavis, L. D.; Raines, R. T. Bright ideas for chemical biology. ACS Chem. Biol. 2008, 3, 142–155.
- (6) Nguyen, B.; Ciuba, M. A.; Kozlov, A. G.; Levitus, M.; Lohman, T. M. Protein environment and DNA orientation affect protein-induced Cy3 fluorescence enhancement. Biophys. J. 2019, 117, 66–73.
- (7) Oliveira, E.; Bértolo, E.; Núñez, C.; Pilla, V.; Santos, H. M.; Fernández-Lodeiro, J.; Fernández-Lodeiro, A.; Djafari, J.; Capelo, J. L.; Lodeiro, C. Green and Red Fluores-

- cent Dyes for Translational Applications in Imaging and Sensing Analytes: A Dual-Color Flag. ChemistryOpen 2018, 7, 9–52.
- (8) Kringle, L.; Sawaya, N. P. D.; Widom, J.; Adams, C.; Raymer, M. G.; Aspuru-Guzik, A.; Marcus, A. H. Temperature-Dependent Conformations of Exciton-Coupled Cy3 Dimers in Double-Stranded DNA. J. Chem. Phys. 2018, 148, 085101.
- (9) Heussman, D.; Kittell, J.; Kringle, L.; Tamimi, A.; von Hippel, P. H.; Marcus, A. H. Measuring Local Conformations and Conformational Disorder of (Cy3)2 Dimer Labeled DNA Fork Junctions Using Absorbance, Circular Dichroism and Two-Dimensional Fluorescence Spectroscopy. Faraday Discuss. 2019, 216, 211–235.
- (10) Lee, T.-H.; Lapidus, L. J.; Zhao, W.; Travers, K. J.; Herschlag, D.; Chu, S. Measuring the folding transition time of single RNA molecules. *Biophys. J.* **2007**, *92*, 3275–3283.
- (11) Hwang, H.; Myong, S. Protein induced fluorescence enhancement (PIFE) for probing protein–nucleic acid interactions. *Chem. Soc. Rev.* **2014**, *43*, 1221–1229.
- (12) Rashid, F.; Raducanu, V.-S.; Zaher, M. S.; Tehseen, M.; Habuchi, S.; Hamdan, S. M. Initial state of DNA-Dye complex sets the stage for protein induced fluorescence modulation. *Nat. Commun.* **2019**, *10*, 1–14.
- (13) Kretschy, N.; Sack, M.; Somoza, M. M. Sequence-dependent fluorescence of Cy3-and Cy5-labeled double-stranded DNA. *Bioconjugate Chem.* **2016**, *27*, 840–848.
- (14) Conley, N. R.; Biteen, J. S.; Moerner, W. Cy3-Cy5 covalent heterodimers for single-molecule photoswitching. *J. Phys. Chem. B* **2008**, *112*, 11878–11880.
- (15) Lee, W.; von Hippel, P. H.; Marcus, A. H. Internally labeled Cy3/Cy5 DNA constructs show greatly enhanced photo-stability in single-molecule FRET experiments. *Nucleic Acids Res.* 2014, 42, 5967–5977.

- (16) Phelps, C.; Lee, W.; Jose, D.; von Hippel, P. H.; Marcus, A. H. Single-molecule FRET and linear dichroism studies of DNA breathing and helicase binding at replication fork junctions. Proc. Natl. Acad. Sci. U.S.A. 2013, 110, 17320–17325.
- (17) Hillisch, A.; Lorenz, M.; Diekmann, S. Recent advances in FRET: distance determination in protein–DNA complexes. *Curr. Opin. Struct. Biol.* **2001**, *11*, 201–207.
- (18) Jones, G.; Bradshaw, D. Resonance energy transfer: from fundamental theory to recent applications. *Front. Phys.* **2019**, *7*, 100.
- (19) Scholes, G. D. Long-range resonance energy transfer in molecular systems. *Annu. Rev. Phys. Chem.* **2003**, *54*, 57–87.
- (20) Cantor, C. R.; Schimmel, P. R. Biophysical chemistry: Part II: Techniques for the study of biological structure and function; Macmillan, 1980.
- (21) Dahlbom, M.; Pullerits, T.; Mukamel, S.; Sundström, V. Exciton delocalization in the B850 light-harvesting complex: comparison of different measures. J. Phys. Chem. B 2001, 105, 5515–5524.
- (22) Frenkel, J. On the transformation of light into heat in solids. II. *Phys. Rev.* **1931**, *37*, 1276.
- (23) Rindermann, J. J.; Pozina, G.; Monemar, B.; Hultman, L.; Amano, H.; Lagoudakis, P. G. Dependence of resonance energy transfer on exciton dimensionality. Phys. Rev. Lett. 2011, 107, 236805.
- (24) Scholes, G. D.; Ghiggino, K. P. Advances In Multi-Photon Processes And Spectroscopy: (Volume 10); World Scientific, 1996; pp 95–331.
- (25) Kistler, K. A.; Spano, F. C.; Matsika, S. A Benchmark of Excitonic Couplings Derived from Atomic Transition Charges. J. Phys. Chem. B 2013, 117, 2032–2044.

- (26) Hsu, C.-P.; You, Z.-Q.; Chen, H.-C. Characterization of the short-range couplings in excitation energy transfer. *J. Phys. Chem. C* **2008**, *112*, 1204–1212.
- (27) Czader, A.; Bittner, E. R. Calculations of the Exciton Coupling Elements Between the DNA Bases Using the Transition Density Cube Method. J. Chem. Phys. 2008, 128, 5101.
- (28) Krueger, B. P.; Scholes, G. D.; Fleming, G. R. Calculation of couplings and energy-transfer pathways between the pigments of LH2 by the ab initio transition density cube method. J. Phys. Chem. B 1998, 102, 5378–5386.
- (29) Schelter, I.; Kummel, S. Accurate Evaluation of Real-Time Density Functional Theory Providing Access to Challenging Electron Dynamics. J. Chem. Theory Comput. 2018, 14, 1910–1927.
- (30) Jornet-Somoza, J.; Lebedeva, I. Real-time propagation TDDFT and density analysis for exciton coupling calculations in large systems. *J. Chem. Theory Comput.* **2019**, *15*, 3743–3754.
- (31) Madjet, M.; Abdurahman, A.; Renger, T. Intermolecular Coulomb couplings from ab initio electrostatic potentials: application to optical transitions of strongly coupled pigments in photosynthetic antennae and reaction centers. J. Phys. Chem. B 2006, 110, 17268–17281.
- (32) Mulliken, R. S. Electronic population analysis on LCAO–MO molecular wave functions.I. J. Chem. Phys. 1955, 23, 1833–1840.
- (33) Lu, T.; Chen, F. Multiwfn: a multifunctional wavefunction analyzer. *J. Comput. Chem.* **2012**, *33*, 580.
- (34) Sengupta, S.; Ebeling, D.; Patwardhan, S.; Zhang, X.; von Berlepsch, H.; Böttcher, C.; Stepanenko, V.; Uemura, S.; Hentschel, C.; Fuchs, H. et al. Biosupramolecular

- Nanowires from Chlorophyll Dyes with Exceptional Charge-Transport Properties. Angew. Chem. Int. Ed. 2012, 51, 6378–6382.
- (35) Patwardhan, S.; Sengupta, S.; Wurthner, F.; Siebbeles, L. D.; Grozema, F. Theoretical study of the optical properties of artificial self-assembled zinc chlorins. J. Phys. Chem. C 2010, 114, 20834–20842.
- (36) Fujimoto, K. J. Electronic coupling calculations with transition charges, dipoles, and quadrupoles derived from electrostatic potential fitting. J. Chem. Phys. 2014, 141, 214105.
- (37) Scrocco, E.; Tomasi, J. The electrostatic molecular potential as a tool for the interpretation of molecular properties, in New concepts II; Springer, 1973; pp 95–170.
- (38) Chirlian, L. E.; Francl, M. M. Atomic charges derived from electrostatic potentials: A detailed study. *J. Comput. Chem.* **1987**, *8*, 894–905.
- (39) Singh, U. C.; Kollman, P. A. An approach to computing electrostatic charges for molecules. *J. Comput. Chem.* **1984**, *5*, 129–145.
- (40) Breneman, C. M.; Wiberg, K. B. Determining atom-centered monopoles from molecular electrostatic potentials. The need for high sampling density in formamide conformational analysis. *J. Comput. Chem.* **1990**, *11*, 361–373.
- (41) Bayly, C. I.; Cieplak, P.; Cornell, W.; Kollman, P. A. A well-behaved electrostatic potential based method using charge restraints for deriving atomic charges: the RESP model. J. Phys. Chem. 1993, 97, 10269–10280.
- (42) Förster, T. Energy migration and fluorescence. J. Biomed. Opt. 2012, 17, 011002.
- (43) Förster, T. Intermolecular energy transference and fluorescence. *Ann. Phys.* **1948**, *437*, 55–75.

- (44) Förster, T. 1965. Delocalized excitation and excitation transfer. In: Sinanoglu, O, editor. Modern quantum chemistry part III: action of light and organic crystals. New York: Academic Press. p. 93–137.
- (45) Munoz-Losa, A.; Curutchet, C.; Krueger, B. P.; Hartsell, L. R.; Mennucci, B. Fretting about FRET: failure of the ideal dipole approximation. *Biophys. J.* **2009**, *96*, 4779–4788.
- (46) Sobakinskaya, E.; Schmidt am Busch, M.; Renger, T. Theory of FRET "spectroscopic ruler" for short distances: Application to polyproline. *J. Phys. Chem. B* **2018**, *122*, 54–67.
- (47) Abramavicius, D.; Palmieri, B.; Mukamel, S. Extracting single and two-exciton couplings in photosynthetic complexes by coherent two-dimensional electronic spectra. *J. Chem. Phys.* **2009**, *357*, 79–84.
- (48) Lamola, A.; Eisinger, J. On the mechanism of thymine photodimerization. *Proc. Natl. Acad. Sci. U.S.A.* **1968**, *59*, 46.
- (49) Halpin, A.; Johnson, P. J.; Tempelaar, R.; Murphy, R. S.; Knoester, J.; Jansen, T. L.; Miller, R. D. Two-dimensional spectroscopy of a molecular dimer unveils the effects of vibronic coupling on exciton coherences. *Nat. Chem.* 2014, 6, 196–201.
- (50) Duan, H.-G.; Nalbach, P.; Prokhorenko, V. I.; Mukamel, S.; Thorwart, M. On the origin of oscillations in two-dimensional spectra of excitonically-coupled molecular systems. *New J. Phys.* 2015, 17, 072002.
- (51) Hofmann, D.; Körzdörfer, T.; Kümmel, S. Energy transfer and Förster's dipole coupling approximation investigated in a real-time Kohn-Sham scheme. *Phys. Rev. A* **2010**, *82*, 012509.

- (52) Czikklely, V.; Forsterling, H.; Kuhn, H. Extended dipole model for aggregates of dye molecules. *Chem. Phys. Lett.* **1970**, *6*, 207–210.
- (53) Dexter, D. L. A theory of sensitized luminescence in solids. J. Chem. Phys. 1953, 21, 836–850.
- (54) Scholes, G. D.; Ghiggino, K. P. Electronic Interactions and Interchromophore Excitation Transfer. J. Phys. Chem. 1994, 98, 4580–4590.
- (55) You, Z. Q.; Hsu, C. P. Theory and Calculation for the Electronic Coupling in Excitation Energy Transfer. *Int. J. Quantum Chem.* **2014**, *114*, 102.
- (56) Voityuk, A. A. Fragment transition density method to calculate electronic coupling for excitation energy transfer. *J. Chem. Phys.* **2014**, *140*, 244117.
- (57) Wong, C. Y.; Curutchet, C.; Tretiak, S.; Scholes, G. D. Ideal dipole approximation fails to predict electronic coupling and energy transfer between semiconducting single-wall carbon nanotubes. *J. Chem. Phys.* **2009**, *130*, 081104.
- (58) Hestand, N. J.; Spano, F. C. Expanded theory of H-and J-molecular aggregates: the effects of vibronic coupling and intermolecular charge transfer. J. Chem. Rev. 2018, 118, 7069–7163.
- (59) Oleson, A.; Zhu, T.; Dunn, I. S.; Bialas, D.; Bai, Y.; Zhang, W.; Dai, M.; Reichman, D. R.; Tempelaar, R.; Huang, L. et al. Perylene diimide-based hj-and hj-aggregates: The prospect of exciton band shape engineering in organic materials. J. Phys. Chem. C 2019, 123, 20567–20578.
- (60) Fornari, R. P.; Rowe, P.; Padula, D.; Troisi, A. Importance and nature of short-range excitonic interactions in light harvesting complexes and organic semiconductors. J. Chem. Theory Comput. 2017, 13, 3754–3763.

- (61) Janke, S. M.; Qarai, M. B.; Blum, V.; Spano, F. C. Frenkel-Holstein Hamiltonian applied to absorption spectra of quaterthiophene-based 2D hybrid organic-inorganic perovskites. *J. Chem. Phys.* **2020**, *152*, 144702.
- (62) Hu, H.; Lu, Z.; Yang, W. Fitting molecular electrostatic potentials from quantum mechanical calculations. J. Chem. Theory Comput. 2007, 3, 1004–1013.
- (63) Renger, T.; Madjet, M. E.-A.; Am Busch, M. S.; Adolphs, J.; Müh, F. Structure-based modeling of energy transfer in photosynthesis. *Photosynth. Res.* **2013**, *116*, 367–388.
- (64) Pescitelli, G.; Bruhn, T. Good computational practice in the assignment of absolute configurations by TDDFT calculations of ECD spectra. *Chirality* **2016**, *28*, 466–474.
- (65) Pescitelli, G. For a correct application of the CD exciton chirality method: the case of laucysteinamide A. Mar. Drugs 2018, 16, 388.
- (66) López-Tarifa, P.; Liguori, N.; van den Heuvel, N.; Croce, R.; Visscher, L. Coulomb couplings in solubilised light harvesting complex II (LHCII): challenging the ideal dipole approximation from TDDFT calculations. *Phys. Chem. Chem. Phys.* 2017, 19, 18311–18320.
- (67) Abu-Awwad, F.; Politzer, P. Variation of parameters in Becke-3 hybrid exchange-correlation functional. *J. Comput. Chem.* **2000**, *21*, 227–238.
- (68) Galvao, D.; Soos, Z.; Ramasesha, S.; Etemad, S. A parametric method 3 (PM3) study of trans-stilbene. J. Chem. Phys. 1993, 98, 3016–3021.
- (69) Pople, J.; Seeger, R.; Krishnan, R. Variational configuration interaction methods and comparison with perturbation theory. *Int. J. Quantum Chem.* **1977**, *12*, 149–163.
- (70) Lin, Y.-S.; Li, G.-D.; Mao, S.-P.; Chai, J.-D. Long-range corrected hybrid density functionals with improved dispersion corrections. *J. Chem. Theory Comput.* **2013**, *9*, 263–272.

- (71) Dreuw, A.; Wormit, M. The algebraic diagrammatic construction scheme for the polarization propagator for the calculation of excited states. WIREs Comput. Mol. Sci. **2015**, 5, 82–95.
- (72) Pettersen, E. F.; Goddard, T. D.; Huang, C. C.; Couch, G. S.; Greenblatt, D. M.; Meng, E. C.; Ferrin, T. E. UCSF Chimera—a visualization system for exploratory research and analysis. *J. Comput. Chem.* **2004**, *25*, 1605–1612.
- (73) Frisch, M. J.; Trucks, G. W.; Schlegel, H. B.; Scuseria, G. E.; Robb, M. A.; Cheeseman, J. R.; Scalmani, G.; Barone, V.; Petersson, G. A.; Nakatsuji, H. et al. Gaussian~16 Revision C.01. 2016; Gaussian Inc. Wallingford CT.
- (74) Shao, Y.; Gan, Z.; Epifanovsky, E.; Gilbert, A. T.; Wormit, M.; Kussmann, J.; Lange, A. W.; Behn, A.; Deng, J.; Feng, X. et al. Advances in molecular quantum chemistry contained in the Q-Chem 4 program package. *Mol. Phys.* 2015, 113, 184– 215.
- (75) Local version of TURBOMOLE V6.5 2013, a development of University of Karlsruhe and Forschungszentrum Karlsruhe GmbH, 19892007, TURBOMOLE GmbH since 2007.
- (76) Mennucci, B.; Tomasi, J. Continuum solvation models: A new approach to the problem of solute's charge distribution and cavity boundaries. J. Chem. Phys. 1997, 106, 5151– 5158.
- (77) Cossi, M.; Rega, N.; Scalmani, G.; Barone, V. Energies, structures, and electronic properties of molecules in solution with the C-PCM solvation model. *J. Comput. Chem.* **2003**, *24*, 669–681.
- (78) Tomasi, J.; Persico, M. Molecular interactions in solution: an overview of methods based on continuous distributions of the solvent. *Chem. Rev.* **1994**, *94*, 2027–2094.

- (79) Cammi, R.; Tomasi, J. Nonequilibrium solvation theory for the polarizable continuum model: a new formulation at the SCF level with application to the case of the frequency-dependent linear electric response function. *Int. J. Quantum Chem.* **1995**, *56*, 465–474.
- (80) Nicoli, F.; Roos, M. K.; Hemmig, E. A.; Di Antonio, M.; de Vivie-Riedle, R.; Liedl, T. Proximity-Induced H-Aggregation of Cyanine Dyes on DNA-Duplexes. J. Phys. Chem. A 2016, 120, 9941–9947.
- (81) Zakharova, G.; Avakyan, V.; Markelov, V.; Svyatoslavskii, N.; Svyatoslavskaya, T.; Chibisov, A. Effect of cucurbituril on the primary photoprocesses in indocarbocyanine dyes in water. *High Energy Chem.* 2015, 49, 407–414.
- (82) Hayashi-Takanaka, Y.; Stasevich, T. J.; Kurumizaka, H.; Nozaki, N.; Kimura, H. Evaluation of chemical fluorescent dyes as a protein conjugation partner for live cell imaging. *PloS ONE* **2014**, *9*, e106271.
- (83) Roy, R.; Hohng, S.; Ha, T. A practical guide to single-molecule FRET. *Nat. Methods* **2008**, *5*, 507–516.
- (84) Muddana, H. S.; Morgan, T. T.; Adair, J. H.; Butler, P. J. Photophysics of Cy3-encapsulated calcium phosphate nanoparticles. *Nano Lett.* **2009**, *9*, 1559–1566.
- (85) Dreuw, A.; Head-Gordon, M. Single-reference ab initio methods for the calculation of excited states of large molecules. *Chem. Rev.* **2005**, *105*, 4009–4037.
- (86) Send, R.; Valsson, O.; Filippi, C. Electronic excitations of simple cyanine dyes: reconciling density functional and wave function methods. J. Chem. Theory Comput. 2011, 7, 444–455.
- (87) Zhekova, H.; Krykunov, M.; Autschbach, J.; Ziegler, T. Applications of time dependent and time independent density functional theory to the first π to π\* transition in cyanine dyes. J. Chem. Theory Comput. 2014, 10, 3299–3307.

- (88) Momeni, M. R.; Brown, A. Why do TD-DFT excitation energies of BODIPY/aza-BODIPY families largely deviate from experiment? Answers from electron correlated and multireference methods. J. Chem. Theory Comput. 2015, 11, 2619–2632.
- (89) Le Guennic, B.; Jacquemin, D. Taking up the cyanine challenge with quantum tools. *Acc. Chem. Res.* **2015**, *48*, 530–537.
- (90) Sarkar, R.; Boggio-Pasqua, M.; Loos, P.-F.; Jacquemin, D. Benchmarking TD-DFT and wave function methods for oscillator strengths and excited-state dipole moments. J. Chem. Theory Comput. 2021, 17, 1117–1132.
- (91) Gomez-Jeria, J. S. An empirical way to correct some drawbacks of mulliken population analysis. *J. Chil. Chem. Soc.* **2009**, *54*, 482–485.
- (92) Cramer, C. J. Essentials of Computational Chemistry: Theories and Models, 2nd ed.; Wiley, 2004.
- (93) Sobek, J.; Schlapbach, R. Dependence of Fluorescence Quenching of CY3 Oligonucleotide Conjugates on the Oxidation Potential of the Stacking Base Pair. *Molecules* **2020**, *25*, 5369.

## Graphical TOC Entry

